GENETICS

Cellular response to moderate chromatin architectural defects promotes longevity

Ruofan Yu[1], Luyang Sun[1], Yu Sun[1], Xin Han[2]*, Lidong Qin[2], Weiwei Dang[1†]

Changes in chromatin organization occur during aging. Overexpression of histones partially alleviates these changes and promotes longevity. We report that deletion of the histone H3-H4 minor locus *HHT1-HHF1* extended the replicative life span of *Saccharomyces cerevisiae*. This longevity effect was mediated through TOR signaling inhibition. We present evidence for evolutionarily conserved transcriptional and phenotypic responses to defects in chromatin structure, collectively termed the chromatin architectural defect (CAD) response. Promoters of the CAD response genes were sensitive to histone dosage, with *HHT1-HHF1* deletion, nucleosome occupancy was reduced at these promoters allowing transcriptional activation induced by stress response transcription factors Msn2 and Gis1, both of which were required for the life-span extension of *hht1-hhf1*Δ. Therefore, we conclude that the CAD response induced by moderate chromatin defects promotes longevity.

INTRODUCTION

The basic structural unit of a eukaryotic genome, the nucleosome, comprises 146–base pair (bp) DNA segments wrapped around core histones. Proper dynamics of nucleosome formation and higher-level chromatin organization regulate the accessibility of DNA and ensure normal genomic functions (*1*). Thus, histones also function as an indispensable regulatory platform for cellular and biological processes, including aging. Altered histone modifications, which occur during aging, contribute to the aging process (*2*). A decrease in histone protein levels is a hallmark of aging cells (*3*). Overexpression of genes encoding histones H3 and H4 from a galactose-inducible promoter extends the replicative life span (RLS) of the budding yeast, suggesting that histone gene expression capacity may be a limiting factor in aged cells (*4*). However, considering that histone gene expression is cell cycle regulated, the relationship between longevity and histone gene expression dosage cannot be delineated without a careful dosage titration using the native promoters.

Cellular responses to stress, such as starvation, DNA damage, oxidation, and protein aggregation, antagonize aging. The attenuation of these pathways during aging causes accumulation of damaged macromolecules that impair cellular function, while boosting these stress response pathways often promotes longevity. Target of rapamycin (TOR) signaling is a highly conserved regulatory node of cellular stress response, which integrates nutrient and cellular stress signals with cellular metabolism, cell cycle progression, and stress response activation. Starvation or high levels of cellular stress inhibit TOR signaling, leading to the inhibition of protein synthesis and the initiation of the general control protein Gcn4-mediated transcriptional response (*5*). At the chromatin level, there are two distinct changes associated with strong stress signals: Overall transcriptional activity is decreased due to reduced histone acetylation levels and increased chromatin compaction associated with slowed or arrested cell cycle progression, whereas stress response genes are activated by specific transcription factors due to chromatin remodeling at their promoters. However, the response of cells to chromatin-associated changes, especially histone loss, remains poorly understood. Here, we explored the relationship between histone gene expression dosage and longevity in the budding yeast *Saccharomyces cerevisiae* and unexpectedly discovered that moderate reductions in H3-H4 histone gene expression can extend the yeast RLS by activating a distinct stress response and inhibiting the TOR signaling pathway.

RESULTS

Deleting the minor H3-H4–coding gene pair *HHT1-HHF1* extends the RLS

The budding yeast *S. cerevisiae* contains two copies of core histone gene pairs under the control of bidirectional promoters. Despite encoding identical amino acid sequences, the two copies differ in their nucleotide sequences and expression levels. Consistent with a previous report (*6*), *HHT1-HHF1*, the minor H3-H4–coding gene pair, provided approximately 15% of the total H3-H4–encoding mRNA (fig. S1A), whereas the major copy *HHT2-HHF2* accounted for the rest of the H3-H4 transcripts. Although removing both H3-H4 copies is lethal, knockout strains for either gene pair show no observable growth defects (*7*). Deletion of single histone genes disrupted the stoichiometry of nucleosome assembly and reduced the RLS (fig. S1B). Therefore, we genetically manipulated only the complete H3-H4 gene pairs rather than single histone genes. Removal of the minor copy *HHT1-HHF1* (*htf1*Δ), representing 85% of wild-type (WT) H3-H4 dosage, significantly extended the RLS, whereas deletion of *HHT2-HHF2* (*htf2*Δ), cutting down the dosage to 15%, reduced the RLS (Fig. 1A). Consistent with the lack of longevity effects upon *H2A-H2B* overexpression (*4*), deletion of the nonessential H2A-H2B–encoding gene pair had no effect on the life span (Fig. 1B). Reintegrating the deleted copies of *HHT1-HHF1* or *HHT2-HHF2* at the *URA3* locus restored the life span of *htf1*Δ or *htf2*Δ, respectively, to the WT level, suggesting that the life span effects in both deletion strains were the direct result of altered histone gene dosage (Fig. 1, C and D). We ruled out the possibility of Ty transposon–mediated duplication (*8*) in the *htf1*Δ and *htf2*Δ strains by verifying the histone gene copy number via quantitative polymerase chain reaction (qPCR) using genomic DNA (fig. S1C). To further investigate the life-span effects when reducing a histone dosage to between 15 and 85%, we constructed another

[1]Department of Molecular and Human Genetics, and Huffington Center on Aging, Baylor College of Medicine, Houston, TX 77030, USA. [2]Department of Nanomedicine, Houston Methodist Research Institute, Houston, TX 77030, USA.
*Present address: School of Medicine and Life Sciences, Nanjing University of Chinese Medicine, Nanjing, Jiangsu Province, P.R. China, 210023.
†Corresponding author. Email: weiwei.dang@bcm.edu

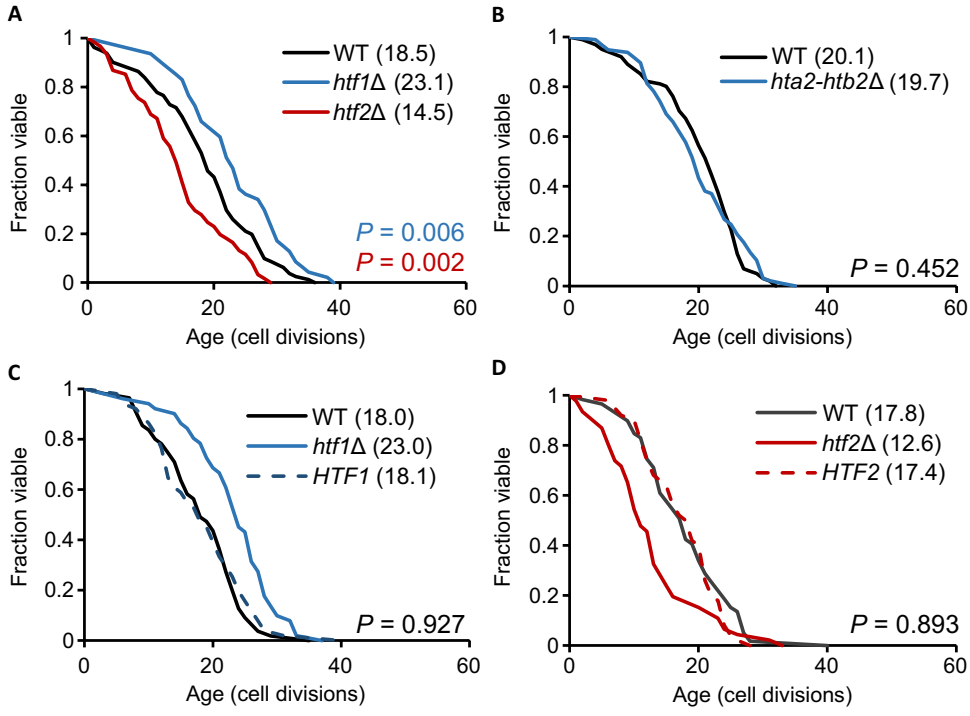

Fig. 1. RLS of histone copy variant strains. (**A**) RLS of the WT ($n = 81$), *htf1*Δ ($n = 51$), and *htf2*Δ ($n = 61$) strains. Values in parentheses on the graph are mean RLS. (**B**) RLS of WT ($n = 101$) and *hta2-htb2*Δ ($n = 97$). (**C**) RLS of WT ($n = 55$) and *htf1*Δ rescue strain *HTF1* ($n = 51$). (**D**) RLS of WT ($n = 59$) and *htf2*Δ rescue strain *HTF2* ($n = 50$).

strain with two copies of *HHT1-HHF1* (*htf2*Δ *HTF1OE*), which provides 30% of WT H3-H4 gene dosage. This strain showed an RLS similar to that of the WT and between those of the *htf1*Δ and *htf2*Δ (fig. S1D), suggesting a dosage-dependent change in life span between 15 and 85% of H3-H4 dosage.

Reduction of the H3-H4 gene copy number increases chromatin accessibility

We next assessed the effect of deleting the histone gene pairs on histone protein levels. In nonsynchronized cells, deletion of either the minor or the major copy of the H3-H4 gene pair had no impact on overall H2B, H3, and H4 protein levels (Fig. 2A), despite the changes in the mRNA levels (Fig. 2B). These observations were similar to a previous report (*9*). Consistent with the findings of reduced histone synthesis capacity in *htf1*Δ and *htf2*Δ, when synchronized, these mutant cells showed significantly lower rates of histone synthesis following the release from α-factor–induced cell cycle arrest (Fig. 2C). Subsequently, we tested whether histone gene deletion affects age-dependent histone depletion. The *htf2*Δ, bearing deletion of the major histone gene copy, showed a greater degree of histone depletion relative to similarly aged *htf1*Δ or WT cells (Fig. 2D and fig. S1E), suggesting that histone synthesis capacity becomes a critical issue in aged cells.

Serving as the building blocks of the nucleosomes, histones greatly affect chromatin architecture. Thus, we assessed histone-dependent effects on chromatin accessibility using micrococcal nuclease (MNase). Young cells of *htf1*Δ and *htf2*Δ strains contained more MNase-accessible chromatin than the WT (Fig. 2E). The *htf2*Δ strain demonstrated a greater increase in chromatin accessibility than *htf1*Δ, commensurate with the respective changes in histone dosages. To further assess local chromatin changes and their effects on transcription of normally silenced regions, we performed RNA sequencing (RNA-seq) to compare the transcriptomes of htf1Δ-, htf2Δ-, and HHT2-HHF2–overexpressing (*HTF2OE*) strains to that of the WT. The subtelomeric genes located within 30 kb of the chromosome ends, which are known to be sensitive to chromatin changes (*10*), were up-regulated in both deletion strains, but not in *HTF2OE* (Fig. 2F), indicating derepression of subtelomeric chromatin. Another heterochromatic region in the budding yeast includes the hidden mating-type loci *HML* and *HMR*, containing silenced copies of mating-type genes *MAT*α and *MAT*a, respectively. Both of the histone gene deletion strains exhibited derepression of the *HML* loci, as evidenced by increased expression of *HMLα1* and decreased sensitivity to the mating pheromone α-factor (Fig. 2, G and H). These changes, however, were not observed in *HTF2OE*. These data indicated a more open chromatin structure in strains with histone gene deletions.

It is particularly interesting that, with the deletion of different histone copies, *htf1*Δ and *htf2*Δ show markedly different life span. Since we observed that knockout of major histone copy leads to substantial chromatin opening (Fig. 2, E and G) compared to *htf1*Δ, we propose that this may lead to a more disturbed transcriptome. The RNA-seq analysis indeed detected more changes in the transcriptome of *htf2*Δ compared to *htf1*Δ, indicating that the extensive loss of histones in this strain leads to higher transcriptional noise (fig. S2A) and may eventually result in the short-lived phenotype. Note that the transcriptome profiles of *htf1*Δ and *htf2*Δ are highly similar, with just a few genes differentially expressed in one mutant but not the other (fig S2B). This fact suggests that deletion of minor or major H3-H4–coding gene leads to similar transcriptional response, while the level of this disturbance is the determinant of life span.

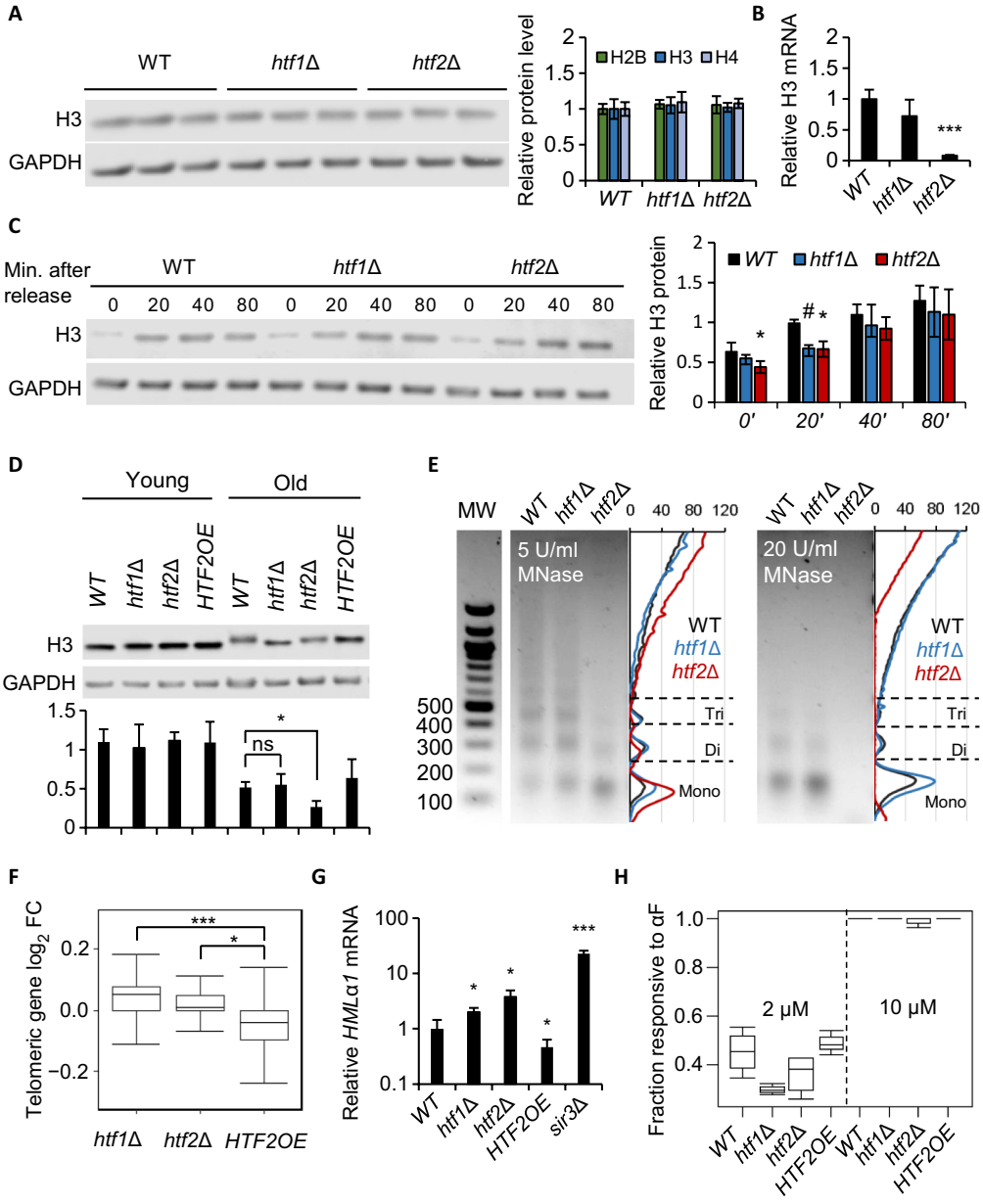

Fig. 2. Reduction in H3-H4 gene copies increases chromatin accessibility. (**A**) Steady-state level of H3 protein, with glyceraldehyde phosphate dehydrogenase (GAPDH) as a loading control (left). No differences in H2B, H3, and H4 levels were found (right). Error bars here and below represent SD, unless noted otherwise. (**B**) qPCR analysis of H3 transcript abundance normalized against H2B transcript level. ***$P < 0.001$ compared to WT. (**C**) H3 protein levels in synchronized cells at indicated times following α-factor release. *$P < 0.05$ and #$P < 0.001$ compared to WT. (**D**) H3 protein levels in old and young cells. *$P < 0.5$; ns, not significant compared to WT. (**E**) MNase digestion assay with designated concentration of MNase. (**F**) Fold change (log_2 FC) in expression of telomeric and subtelomeric genes in *htf1Δ*, *htf2Δ*, and HTF2OE strains. Error bars represent the 25 and 75% percentiles. (**G**) qPCR analysis of *HMLα1* transcript abundance. *$P < 0.05$ and ***$P < 0.001$ compared to WT. (**H**) α-Factor (αF) sensitivity test. Error bars represent the 25 and 75% percentiles.

Given that overexpression of either H3-H4–coding gene pair extends the RLS (fig. S2C) (*4*), we asked whether shared underlying mechanisms exert the anti-aging effects in *htf1Δ* and the histone gene overexpression strains. The Pearson correlation between the transcriptomic patterns of *htf1Δ* and *HTF2OE* was substantially lower than that between the transcriptomes of *htf1Δ* and *htf2Δ* (fig. S2, B and D). In contrast to *htf1Δ*, the overexpression strain also showed no loss of subtelomeric gene or *HML* locus silencing (Fig. 2, F and G). Furthermore, we found that the deletion of the histone transcription regulator 1 (*HIR1*) gene, which by itself increases H3-H4 levels and mimics the H3-H4 overexpression phenotype (*4*), reduced the RLS when combined with deletion of the minor H3-H4 gene pair (*htf1Δ hirΔ*; fig. S2E). These data suggested that the life-span extension mechanism of histone overexpression is likely distinct from what we see in *htf1Δ* cells.

Life-span extension in *htf1Δ* is mediated through the TOR pathway

To determine whether the RLS extension of *htf1Δ* is mediated through known aging regulatory pathways, we performed epistasis analyses. Considering that the aging regulator Sir2 is a chromatin modifier

(*11*), we tested whether it is required for the longevity of the *htf1*Δ cells. The *sir2*Δ single mutant has extremely short life span due to the dominant ribosomal DNA instability (*12*), we tested Sir2 epistasis in a *sir2*Δ *fob1*Δ strain that shows a life span close to the WT. As shown in Fig. 3 (A and B), *htf1*Δ extended life span in the *sir2*Δ *fob1*Δ background, as well as the *SIR2* overexpression background, suggesting that the life span–extending effect of *HHT1-HHF1* deletion is completely independent of the Sir2-Fob1 pathway.

Another well-recognized and evolutionarily conserved aging regulatory pathway is the TOR. The key component of the TOR pathway is the kinase Tor1, which integrates nutrient signaling and cellular stress to elicit global downstream metabolic changes and stress response pathways (*13*) . We found negative epistasis between *tor1*Δ and *htf1*Δ in RLS effects: Despite the extended life spans of the single mutants, the double mutant had a life span similar to that of the single mutants, with no further RLS increase (Fig. 3C). To verify this

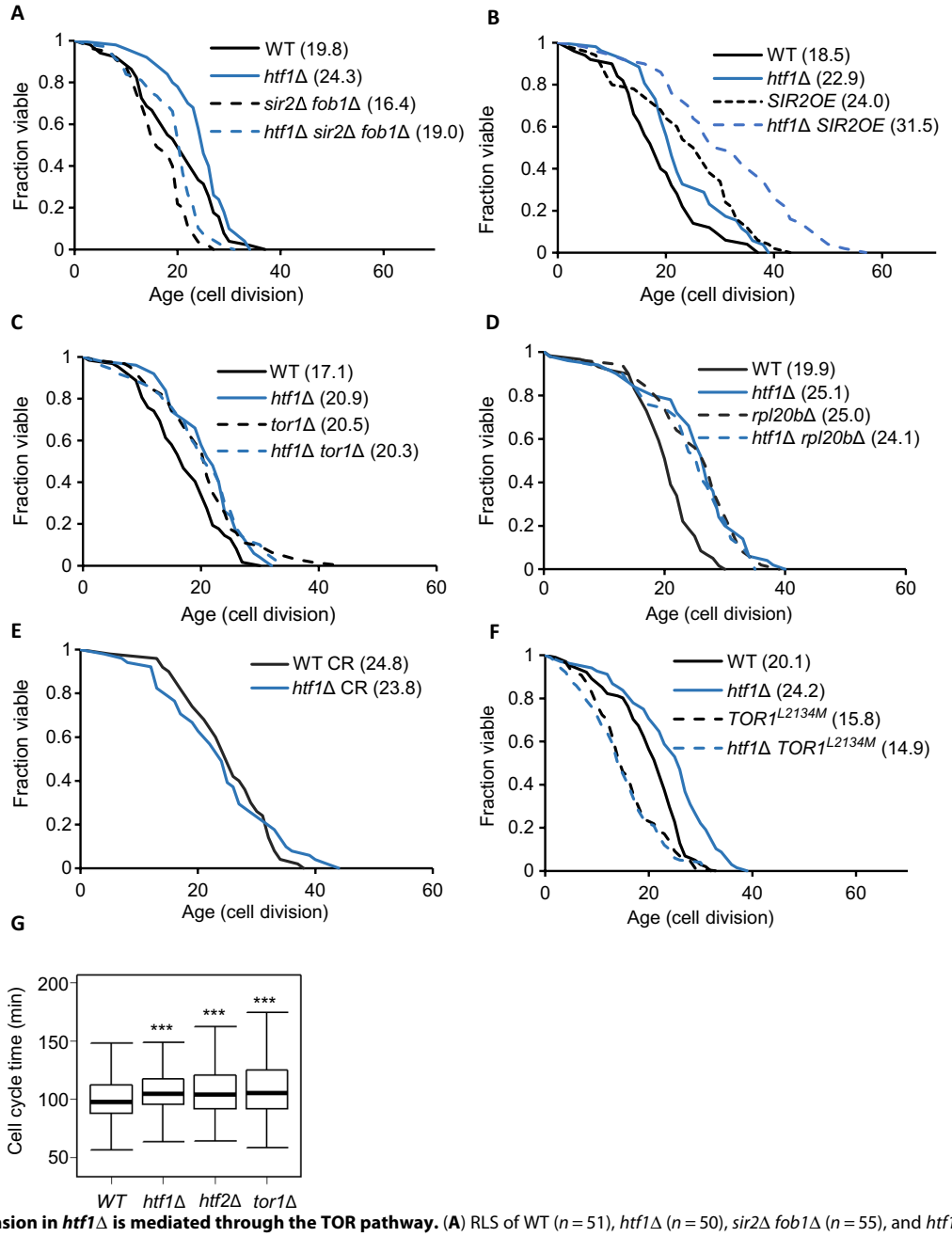

Fig. 3. Life-span extension in *htf1*Δ is mediated through the TOR pathway. (**A**) RLS of WT ($n = 51$), *htf1*Δ ($n = 50$), *sir2*Δ *fob1*Δ ($n = 55$), and *htf1*Δ *sir2*Δ *fob1*Δ ($n = 68$). (**B**) RLS of WT ($n = 50$), *htf1*Δ ($n = 52$), *SIR2OE* ($n = 50$), and *htf1*Δ *SIR2OE* ($n = 50$). (**C**) RLS of WT ($n = 62$), *htf1*Δ ($n = 50$), *tor1*Δ ($n = 63$), and *htf1*Δ *tor1*Δ ($n = 50$). (**D**) RLS of WT ($n = 59$), *htf1*Δ ($n = 50$), *rpl20b*Δ ($n = 50$), and *htf1*Δ *rpl20b*Δ ($n = 50$). (**E**) RLS of WT ($n = 50$) and *htf1*Δ ($n = 50$) cells under caloric restriction (CR; 0.05% glucose), $P = 0.455$. (**F**) RLS of WT ($n = 101$), *htf1*Δ ($n = 68$), $TOR1^{L2134M}$ ($n = 87$), and *htf1*Δ $TOR1^{L2134M}$ ($n = 100$). (**G**) Average cell cycle duration of WT, *htf1*Δ, *htf2*Δ, and *tor1*Δ. ***$P < 0.001$ compared to WT. Error bars represent the 25 and 75% percentiles.

epistatic relationship, we performed similar life-span analysis using either the *rpl20b*Δ strain, which mimics the effects of TOR inhibition (*14*), or calorie restriction conditions. In both cases, *HHT1-HHF1* deletion failed to further extend the life span (Fig. 3, D and E). Furthermore, when introduced into a hyperactive Tor1 mutant, $TOR1^{L2134M}$ (*15*), the *HHT1-HHF1* deletion failed to extend the life span (Fig. 3F), underscoring that inhibition of TOR signaling is required for longevity induced by altered histone dosage. Moreover, the histone mutants and *tor1*Δ have similar growth phenotypes, with slower cell cycles compared to the WT (Fig. 3G).

We reasoned that if TOR signaling is inactivated in *htf1*Δ, then deletion of *HHT1-HHF1* and inhibition or ablation of TOR signaling should induce similar transcriptional responses. Therefore, we used RNA-seq to compare the transcriptomes of *htf1*Δ and *htf2*Δ mutants, calorie-restricted WT cells, and *TOR1*-deleted cells. Gene ontology (GO) analysis revealed categories of genes, including glycolysis and translation, that were similarly down-regulated in histone dosage mutants and calorie-restricted cells (Fig. 4A and fig. S3, A and B) (*16*). Further RNA-seq analysis revealed a substantial number of genes that were similarly down-regulated in *htf1*Δ and *tor1*Δ cells (Fig. 4B). Together, these data supported the hypothesis that TOR signaling inhibition mediates the longevity effect in *htf1*Δ cells.

Stress experienced by the histone deletion strains is distinct from replication or mitotic stress

The *htf1*Δ cells demonstrated up-regulation of genes belonging to GO categories that have been previously linked to stress responses (Fig. 4C), including transposable (*17*) element, proteolysis (*18*), the tricarboxylic acid (TCA) cycle (*19*), and cell wall components (*20*); *htf2*Δ also shows up-regulation of similar categories (fig. S3C). Moreover, we observed a significant overlap between genes up-regulated in *htf1*Δ and those induced by stress (Fig. 4D). Defects in chromatin

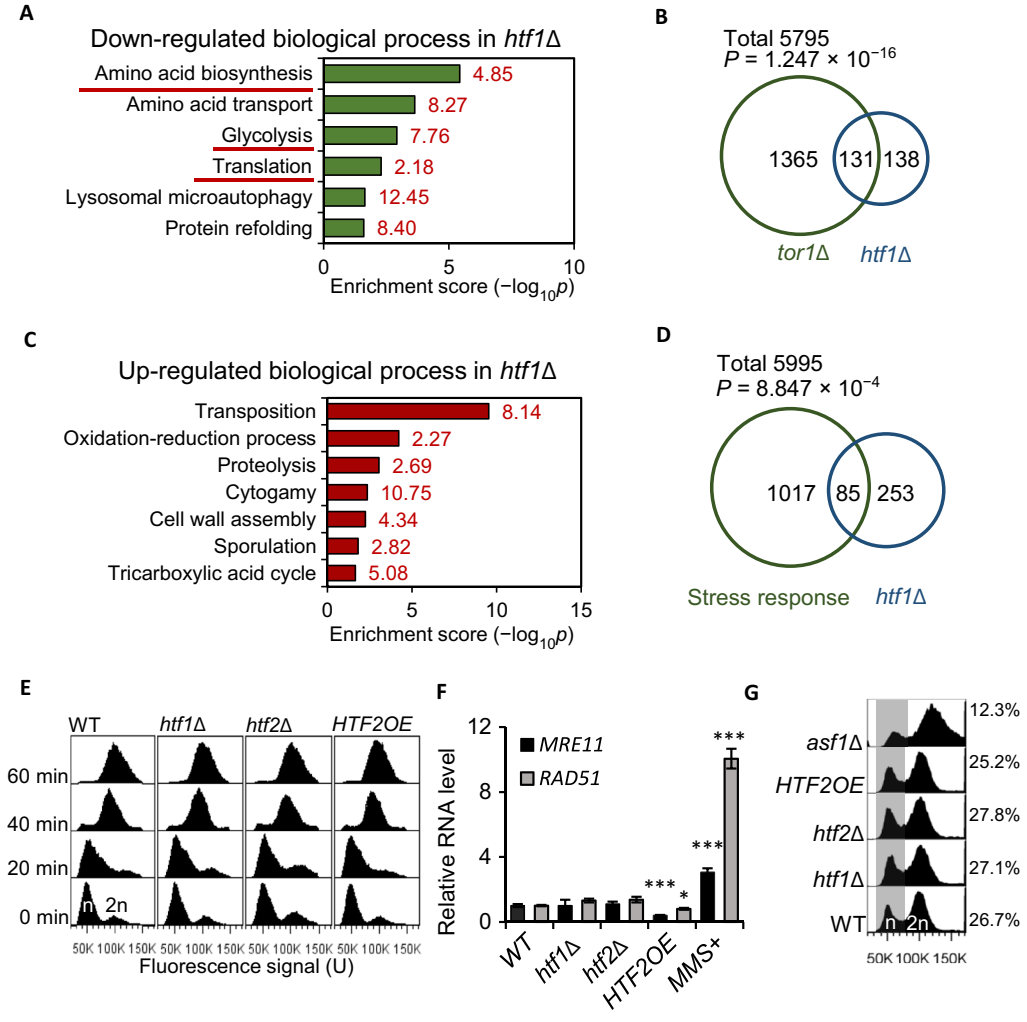

Fig. 4. Transcriptome analysis of histone deletion strains and characterization of stress-related features. (**A**) GO analysis of down-regulated genes in *htf1*Δ. GO categories with Benjamini $P < 0.05$ were included here and in GO analyses below. Underlined categories are enriched in transcriptomic changes of *htf1*Δ and cells under CR. Numbers in all GO figures indicate fold enrichment of the corresponding category. (**B**) Venn diagram showing genes down-regulated in *tor1*Δ cells (total, 1496), in *htf1*Δ cells (total, 269), and in both (total, 131). (**C**) GO analysis of genes up-regulated in *htf1*Δ. (**D**) Overlap between stress-related category genes and genes up-regulated in *htf1*Δ. (**E**) Flow cytometry–based cell cycle analysis of indicated strains. Cells were synchronized with α-factor. (**F**) qPCR analysis of *MRE11* and *RAD51* transcript abundance. *$P < 0.05$ and ***$P < 0.001$ compared to WT. (**G**) Flow cytometry–based cell cycle analysis of indicated strains. Cells were unsynchronized. Percent values represent fraction of cells within the shaded region containing 1N genome.

assembly due to mutations in the histone chaperone chromatin assembly factor 1 (CAF-1) complex cause replication stress, manifested by S phase arrest and DNA damage (*21*). We thus asked whether reduced histone supplies pose similar challenges to DNA replication. However, we did not observe slowed cell cycle progression or stalled S phase in either of the histone deletion strains (Fig. 4E). The histone deletion strains also did not exhibit sensitivity to DNA damaging agents such as hydroxyurea, methyl methanesulfonate (MMS), or phleomycin that cause replication stress (fig. S3D). Furthermore, in contrast to the MMS treatment, inactivation of either of the H3-H4 gene pairs did not induce expression of the genes encoding the replication stress sensor Mre11 (*22*) and the DNA damage responder Rad51 (Fig. 4F) (*23*). These data suggested that the histone dosage mutants do not experience DNA damage and replication stress.

Given that functional chromatin is also essential for separation of sister chromatids during cell division, we next assessed the histone deletion strains for potential mitotic stress. Deletion of the histone chaperone *ASF1* gene causes cells to arrest in the G_2/M phase (*24*), corresponding to a profound decrease in the haploid cell fraction. However, this phenotype was not evident in either the *htf1*Δ or the *htf2*Δ strain (Fig. 4G). The lack of mitotic stress in the histone deletion strains was also underscored by their insensitivity to benomyl, a drug that disrupts microtubule formation and causes mitotic stress (fig. S3D). A recent study of *Caenorhabditis elegans* reported that a decrease in histone levels induces the mitochondrial unfolded protein response (UPR^{mt}) to promote life-span extension (*25*). Hence, we assessed UPR^{mt} induction in the yeast histone deletion mutants. Induction of UPR^{mt} corresponds to the activation of mitochondrial heat shock proteins (HSPs) (*25*), such as Hsp60 and Hsp10 (*26*). Neither of these mitochondrial HSPs was up-regulated in the *htf1*Δ and *htf2*Δ strains according to RNA-seq analysis (fig. S3E). Therefore, the form of stress experienced by the histone deletion mutants was distinct from the above well-characterized stress states.

Disruptions in chromatin architecture trigger a distinct type of stress response

Responses to various stresses can trigger nucleosome position–dependent alterations in chromatin structure and consequent changes in gene transcription (*27*). However, these chromatin changes, especially those occurring during aging, have never been shown to trigger stress responses. Our present data suggest that reduced histone dosage induces a distinct type of stress response. We next asked whether such a stress response can also be observed in other mutants with chromatin alterations. Disruptions of histone- and chromatin-related factors have negative impacts on yeast and higher eukaryotes, inducing chromosomal rearrangement, promoting genome instability, and potentially leading to diseases such as cancer (*28*, *29*). Mutations affecting chromatin regulators, such as the Snf2 family chromatin remodeling enzymes and histone chaperones, result in common phenotypic manifestations: increase in adenosine triphosphate (ATP) biosynthesis and mitochondrial biogenesis accompanied by induction of genes involved in the TCA cycle (*30*). Hence, we tested whether the histone dosage mutants also exhibit these phenotypes. Elevated cellular ATP levels (Fig. 5A) and higher mitochondrial DNA copy numbers (Fig. 5B) were detected in both histone gene pair deletion strains, although to a lesser extent compared with histone chaperone deficient strain *msi1*Δ, *rtt106*Δ, and *asf1*Δ. Moreover, as indicated by the transcriptomic analysis, TCA cycle–related genes were significantly up-regulated in *htf1*Δ cells (Fig. 4C), indicating potentially up-regulated respiration functions.

To further investigate the similarities in the metabolic phenotypes of the histone and chromatin factor mutant strains, we compared the changes in their transcriptomes. There was a significant overlap in the genes differentially regulated in *htf1*Δ and in a strain depleted of H3 (Fig. 5C) (*31*). For a more comprehensive examination, we performed a correlation analysis using the transcriptome of the *hft1*Δ mutant and a recently published dataset containing transcriptomic data for 697 transcriptional responsive single gene deletion yeast strains (*32*). The Pearson correlation between the transcriptomes of *htf1*Δ and every deletion strain in the dataset was calculated and ranked (see Fig. 5D for the top correlated strains and table S3 for complete list). Among those with the highest similarity to *htf1*Δ ($R \geq 0.20$), strains with chromatin factor deletions were significantly enriched ($P < 10^{-6}$, χ^2 test). The highest-ranked mutants included strains inactivated in all three subunits of the CAF-1 complex (Rlf1, Cac2, and Msi1) and in Rtt106, all of which are essential players in DNA replication–dependent nucleosome assembly. We also observed a significant overlap in the genes up-regulated in *hft1*Δ and these mutants (fig. S3, F and G). Together, these data suggested that defects in either histone expression or chromatin regulating factors elicit a similar cellular response, manifested by transcriptomic and metabolic changes, which we collectively refer to as the chromatin architectural defect (CAD).

CAD stress induces a conserved response in different eukaryotic models

Nucleosome and chromatin structures are highly evolutionarily conserved. We thus asked whether the CAD response was conserved in higher eukaryotes as well. We compared the transcriptome of a *Drosophila melanogaster* strain with reduced histone gene copies (*33*) to age- and tissue-matched WT samples (*34*). Consistent with the changes observed here for *htf1*Δ and previously reported for TOR inactivation (*35*), genes associated with translation were significantly down-regulated in the fly histone mutant strain (Fig. 5E). For mammalian cell comparisons, we analyzed an RNA-seq dataset for mouse embryonic stem (MES) cells with a knockdown of p150, which represents the largest catalytic subunit in the CAF-1 histone chaperone complex (*36*). In a manner similar to the histone gene inactivation in *htf1*Δ, defects in CAF-1 in the MES cells resulted in the down-regulation of genes associated with ribosome biogenesis, protein translation, and amino acid biosynthesis (Fig. 5F). Using a published RNA-seq dataset for MES cells treated with the mammalian TOR inhibitor INK128 (*37*), we also detected an overlap in the 1000 most down-regulated genes resulting from TOR pathway inhibition and CAF-1 complex disruption (Fig. 5G). During the preparation of this manuscript, knockdown of H2A expression was found to extend the life span of *C. elegans* (*25*). Transcriptomic analysis of the H2A knockdown worm also revealed significant down-regulation of translation-related processes (Fig. 5H). Thus, inhibition of the TOR pathway in response to CAD stress is likely a conserved phenomenon among eukaryotes. Despite greater, likely organism-specific, differences between the up-regulated gene categories in the analyzed transcriptomes, we did detect comparable up-regulation of genes related to proteolysis and oxidation-reduction in the yeast and MES transcriptomes (Fig. 5 I and J). These observations suggest possible conservation of the CAD response in other eukaryotic organisms.

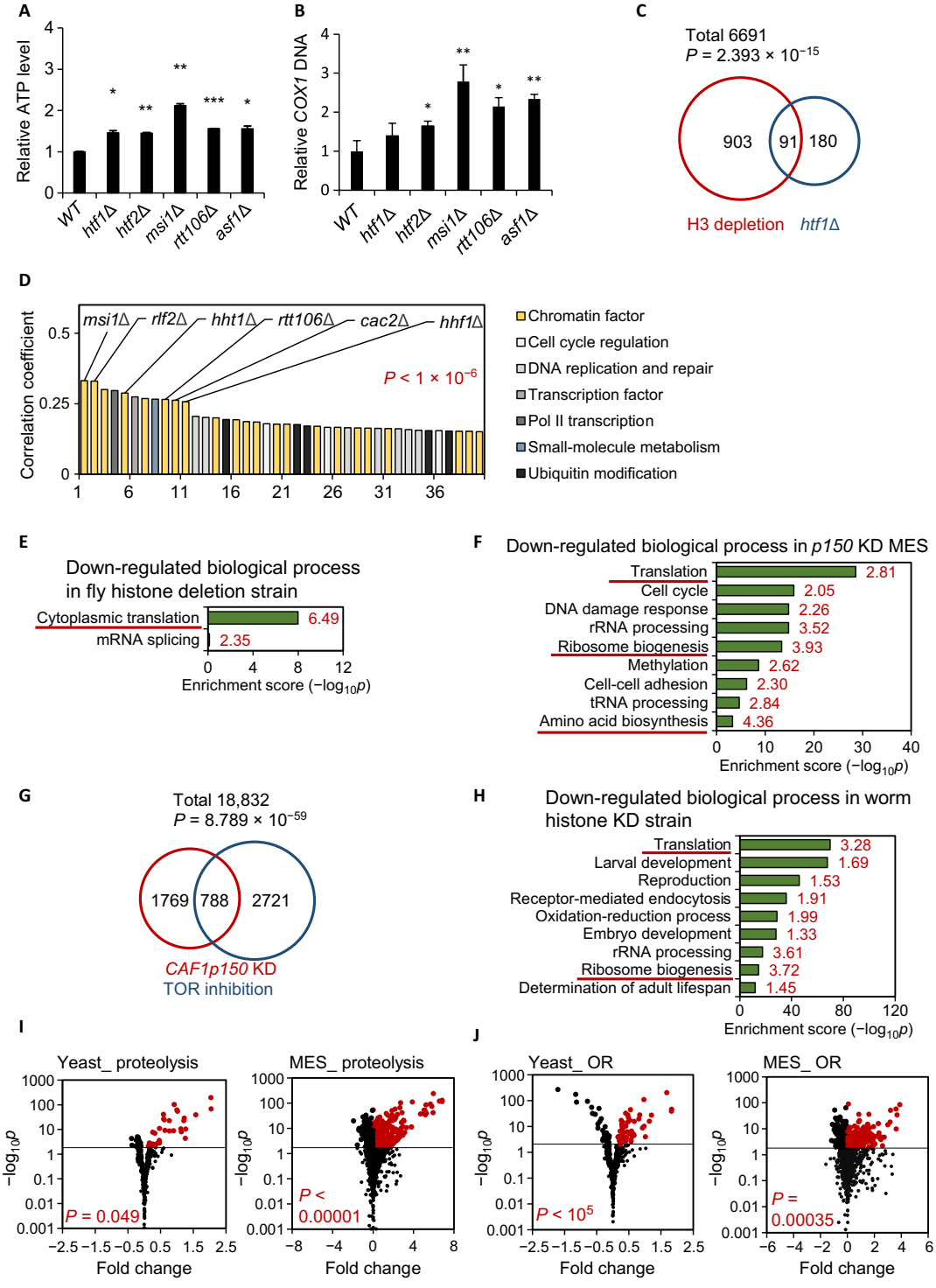

Fig. 5. Similarities between transcriptomic responses and metabolic phenotypes of *htf1*Δ, *htf2*Δ, and other chromatin regulator mutants. (**A**) Relative ATP level in indicated strains. *$P < 0.05$, **$P < 0.01$, and ***$P < 0.001$ compared to WT. (**B**) *COX1* copy number analysis by qPCR in indicated strains. *$P < 0.05$ and **$P < 0.01$ compared to WT. (**C**) Overlap in genes significantly down-regulated in H3 depletion and *htf1*Δ strains. (**D**) Deletion strains with transcriptomes demonstrating the highest-ranking correlations with the *htf1*Δ transcriptome. Names are provided for strains with defects in chromatin-related factors. Genes targeted by the deletion mutations are color-coded according to their molecular function. (**E**) GO analysis of genes down-regulated in a histone knockout fly strain. Categories expected to be affected by TOR inhibition are underlined. (**F**) GO analysis of genes down-regulated in *CAF-1 p150* knockdown MES cells. Categories expected to be affected by TOR inhibition are underlined. (**G**) Down-regulated genes overlapping between *CAF-1 p150* KD and INK128-treated cells. (**H**) GO analysis of genes down-regulated in an *H2A* knockdown worm. Categories expected to be affected by TOR inhibition are underlined. tRNA, transfer RNA. (**I** to **J**) Volcano plots showing up-regulation of proteolysis-related and oxidation-reduction (OR)–related genes in *htf1*Δ yeast cells and *CAF-1 p150* KD MES cells. Red dots represent genes with significantly (false discovery rate < 0.01) up-regulated expression level. KD, knockdown.

Stress response transcription factors connect the CAD response to longevity

We next sought to determine how chromatin changes can induce the CAD stress response and inhibit the TOR pathway. A previous study (*31*) found that histone depletion in yeast primarily causes nucleosome reduction at promoter regions. Another study proposed that the promoters of genes with higher transcriptional plasticity tend to have higher nucleosome occupancy than those of constitutively expressed genes (*27*), leading to the classification of genes as occupied proximal-nucleosome or depleted proximal–nucleosome genes. Such nucleosome positioning provides a mechanism for regulating gene expression in response to environmental cues. Considering these studies, we assessed whether the promoters of genes activated in response to CAD experienced reduced nucleosome occupancy caused by a change in chromatin structure. Using MNase sequencing (MNase-seq), we assayed the global changes in nucleosome occupancy in the *htf1*Δ and *htf2*Δ histone deletion strains. As expected, we found reduced nucleosome occupancy at promoters of several CAD response genes (fig. S4A). To minimize the variance of nucleosome pattern caused by MNase digestion condition in different experiments, we used a permutation test and proved that this reduction is statistically significant in nucleosome occupancy across the promoter regions (defined as −250 to +50 bp relative to the transcription start site) of CAD response genes up-regulated in *htf1*Δ, in both *htf1*Δ and *htf2*Δ background (Fig. 6A and fig. S4B), linking the shared transcriptional response in these two histone deletion strains to shared changes in chromatin structure.

To gain more insight into the promoter properties of CAD response genes, we performed promoter motif analysis and found that the TATA box was significantly enriched in the promoters of the CAD response genes up-regulated in *htf1*Δ (fig S4C). These observations are consistent with previous reports of TATA box–containing promoters contributing to high plasticity of gene expression (*38*). Consistent with this idea, there was a significant decrease in promoter nucleosome occupancy among all stress response genes in *htf1*Δ (Fig. 6B, stress response gene list includes all genes in GO:0009628 response to abiotic stimulus and GO:0006950 response to stress). To further investigate the common modulators of up-regulated genes in the long-lived *htf1*Δ strain, we determined the transcription factors, the targets of which were enriched among these up-regulated genes (table S4). These regulators are likely responsible for activating transcription when their target gene promoters become more open in response to the CAD stress. Many of the identified transcriptional factors, including Msn2, Msn4, and Gis1, are known to be involved in stress response (*39*). Furthermore, the target promoters of Msn2 and Gis1 (fig. S4, D and E) showed significantly lower nucleosome occupancy in *htf1*Δ, supporting that these transcriptional regulators likely activate their target genes under conditions of CAD stress.

To investigate the transcriptional regulation by Msn2 and Gis2 in response to CAD stress, we clustered the transcriptomes of 697 responsive mutants from (*32*) using the 134 Msn2- and Gis1-regulated genes significantly up-regulated in *htf1*Δ (table S5). Cluster 2 (fig. S4F) contained a significant enrichment of chromatin factors, indicating that the targets of Msn2 and Gis1 represent a common set of genes induced by different factors that cause CAD stresses.

We reasoned that if these transcription factors mediate longevity in *htf1*Δ, then there should be an epistatic relationship in the regulation of RLS between the respective genes. Deletion of *MSN2*, *MSN4*, or *GIS1* reduced the life span of *htf1*Δ nearly to the WT level (Fig. 6, C and D, and fig. S4G). As a negative control, deletion of *HOT1*, another significantly enriched transcription factor, did not reduce the increased RLS of *htf1*Δ (fig. S4H). Overexpression of Msn2 could not extend RLS or abrogate the longevity phenotype of *htf1*Δ (Fig. 6E), whereas Gis1 overexpression significantly extend RLS and showed epistasis with *htf1*Δ (Fig. 6F), indicating that Gis1 may have a more direct role in *htf1*Δ-dependent longevity. This observation is understandable because Gis1 targets are most significantly enriched in genes up-regulated in *htf1*Δ (table S4). Furthermore, deletion of *MSN2* or *GIS1* in *htf1*Δ significantly reduced the expression levels of CAD-induced genes, including *YGP1*, *ADH2*, *NQM1*, and *YRO2* (Fig. 6G). Reduction of CAD-induced genes expression, however, was not elicited by the Tor1 hyperactive $TOR1^{L2134M}$ mutation. These results suggested that life-span extension following *HHT1-HHF1* deletion requires Msn2/Gis1-dependent induction of CAD response genes and that TOR inhibition is downstream of the transcriptional activation in response to CAD stress.

DISCUSSION

Chromatin is involved in the modulation of most eukaryotic cellular processes through its role in transcriptional regulation. Epigenetic marks in chromatin and ATP-dependent chromatin remodeling, which are affected by aging, contribute to the regulation of longevity (*2*). In this study, we investigated the relationship between histone H3-H4 gene expression dosage and longevity using mutant strains with graduated histone gene expression driven by native promoters. Unexpectedly, we found that moderately reducing histone gene expression by deleting the minor copy of the H3-H4–coding genes *HHT1-HHF1* extended yeast RLS in a TOR-dependent manner. Cells with reduced histone gene expression exhibited many phenotypic manifestations and transcriptional responses similar to those observed in cells with CADs, such as histone chaperone and chromatin factor mutant strains. We found that the promoters of genes activated by chromatin stress showed significantly reduced nucleosome occupancy when histone dosage was decreased. Furthermore, we identified stress response transcription factors, namely, Msn2, Msn4, and Gis1 that mediated not only the transcriptional responses but also the longevity phenotype of the minor H3-H4 copy deletion strain (Fig. 6F). These transcriptional responses were independent of TOR inhibition. Thus, transcriptional activation in response to moderate chromatin stress likely leads to TOR inhibition, which, in turn, induces further downstream transcriptional and translational responses, eventually promoting longevity (Fig. 6H).

Molecular and phenotypic effects of reduced histone dosage

Because of their importance in cell function and survival, histones have evolved multiple redundancy mechanisms (*40*). Deletion of either of the copies of the H3-H4 genes did not affect growth or histone protein levels in a rich medium (Fig. 2A). Whereas moderate delays in histone synthesis could be detected in synchronized cells (Fig. 2C), significant loss of histone was detected in old cells upon deletion of the major histone gene pair copy (Fig. 2D), commensurate with markedly reduced histone mRNA levels (Fig. 2B). These observations suggested that histone synthesis capacity is in excess of young cells' needs but becomes limiting in old cells. This change may be caused by decreased protein synthesis and/or decreased mRNA stability in aged cells.

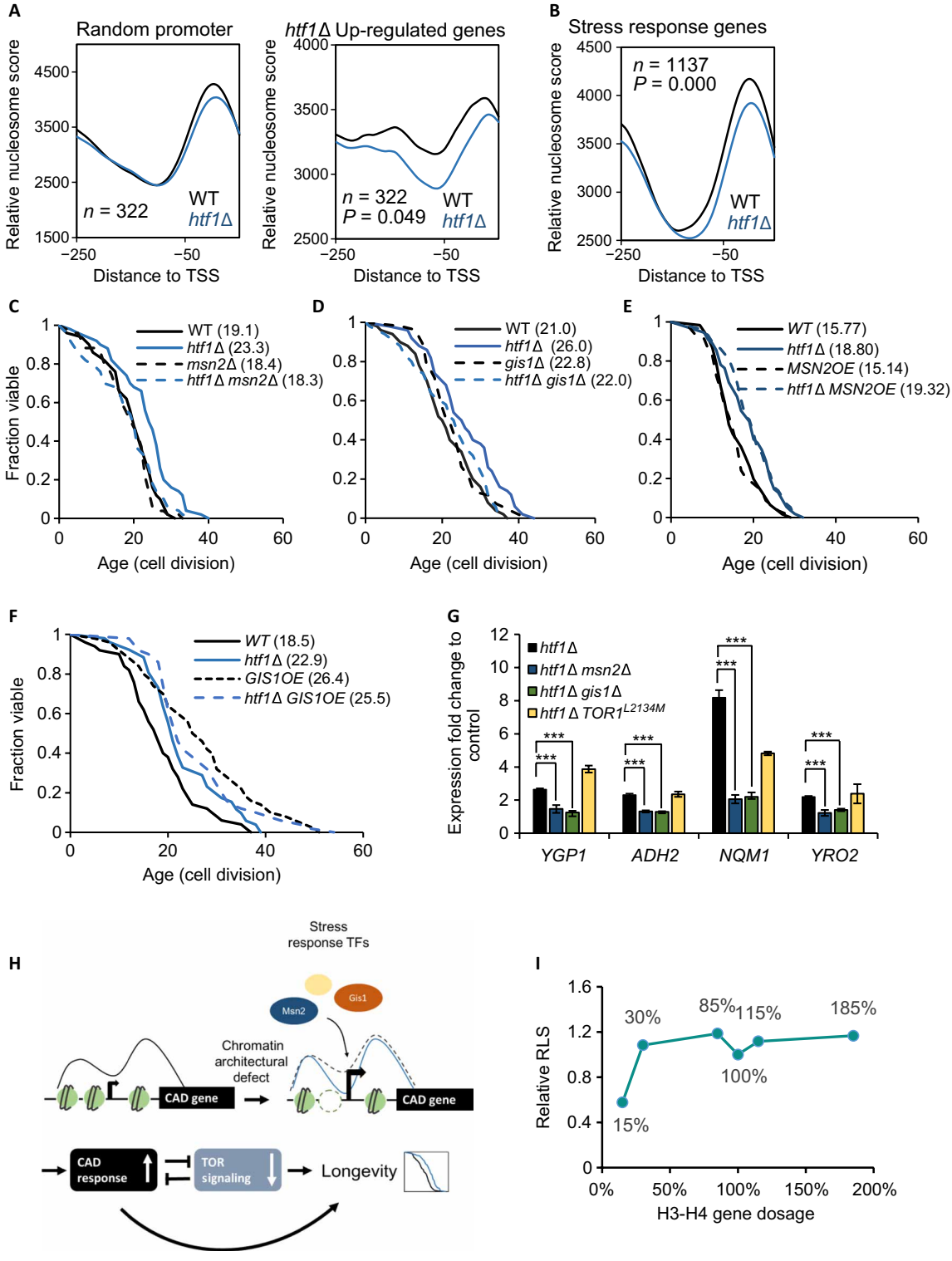

Fig. 6. Stress response factors connect CAD to longevity. (**A**) Nucleosome profiles in WT and *htf1*Δ background cells of randomly picked 322 genes promoter regions (left). Nucleosome profiles of promoters of genes significantly up-regulated in *htf1*Δ (right). *n*, number of genes in the designated category. (**B**) Nucleosome profile of promoters of all yeast stress response genes as listed in table S2. (**C**) RLS of WT ($n = 50$), *htf1*Δ ($n = 50$), *msn2*Δ ($n = 51$), and *htf1*Δ *msn2*Δ ($n = 50$). (**D**) RLS of WT ($n = 50$), *htf1*Δ ($n = 50$), *gis1*Δ, ($n = 50$), and *htf1*Δ *gis1*Δ ($n = 50$). (**E**) RLS of WT ($n = 61$), *htf1*Δ ($n = 55$), *MSN2OE* ($n = 58$), and *htf1*Δ *MSN2OE* ($n = 58$). (**F**) RLS of WT ($n = 50$), *htf1*Δ ($n = 52$), *GIS1OE* ($n = 50$), and *htf1*Δ *GIS1OE* ($n = 50$). (**G**) Transcript levels of designated genes were measured by qPCR and normalized to the corresponding background: *htf1*Δ to WT, *htf1*Δ *msn2*Δ to *msn2*Δ, *htf1*Δ *gis1*Δ to *gis1*Δ, *htf1*Δ $TOR1^{L2134M}$ to $TOR1^{L2134M}$. ***$P < 0.001$ compared to *htf1*Δ single deletion. (**H**) Model of CAD-dependent longevity. (**I**) Correlation between H3-H4 gene dosage and RLS obtained from this study. TSS, transcription start site.

Table 1. Antibodies used in this study.

Antibody	Source	Identifier
Rabbit anti histone H3	Active motif	61277
Mouse anti histone H3	Active motif	61475
Rabbit anti histone H4	Millipore	04-858
Rabbit anti histone H2B	Abcam	ab1790
Goat anti-Mouse IgG secondary antibody, DyLight 800	Thermo Fisher Scientific	35521
Goat anti-Rabbit IgG secondary antibody, DyLight 680	Thermo Fisher Scientific	35568
Mouse anti-GAPDH	Thermo Fisher Scientific	MA515738

Table 2. Reverse transcription PCR primers used in this study.

Name	Sequence	Source
HHT shared forward	GCAACAGTACCTGGCTTATATCT	This study
HHT shared reverse	CCATCTACCGGTGGTGTTAAG	This study
HHT2 unique reverse	AAAGGAGATGTTTGTATGATGTCC	This study
HHT2 unique forward	GGATATCAAATTGGCCAGAAG	This study
HHT1 unique reverse	TGGCTAGAAGATTAAGAGGTGAAA	This study
HHT1 unique forward	CAACTGTTAAAGAACCCAGTAAACC	This study
HTF1 DNA forward	CTTGCTCTGCACCTTTGCGA	This study
HTF1 DNA reverse	GAGCCGTGGAGGGTACCAAA	This study
HTF2 DNA forward	AGGACGTTCTGGGAGCTTCG	This study
HTF2 DNA reverse	CAGGCGCGAGTGAACAACAT	This study
ACT1 forward	TCGTTCCAATTTACGCTGGTT	This study
ACT1 reverse	CGGCCAAATCGATTCTCAA	This study
HTB shared forward	CCCTGACACTGGTATTTCCC	This study
HTB1 shared reverse	GCTTCAGTAGCGATTCTTTCAA	This study
HMLα1 forward	TCAATATTATTCGACCACTCAAGAAAG	(*15*)
HMLα1 reverse	CGCTATCCTGTGAATTTGGATTT	(*15*)
MRE11 forward	GCGGAAAGCAGTAAGCCAACG	(*15*)
MRE11 reverse	TCGTTGCAGTTCGCACTCGT	(*15*)
RAD51 forward	CCGGTAAGATTGGTATCCATAGCT	(*15*)
RAD51 reverse	CGCAACGTTGTTCAAAGCA	(*15*)
COX1 DNA forward	CAACAAATGCAAAAGATATTGCAG	(*28*)
COX1 DNA reverse	AATATTGTGAACCAGGTGCAGC	(*28*)
YRO2 forward	GCTAAGAAGGCCAAGAAGGC	This study
YRO2 reverse	TCAGAGTCGGTGGCTACATC	This study
NQM1 forward	TGATAAGAAGGCGACGGTGA	This study
NQM1 reverse	TGGATACCCTCCCACGTAGA	This study
ADH2 forward	GATGGTGGTCCAGGAAAGGA	This study
ADH2 reverse	TAGCCTTAACGACTGCGCTA	This study
YGP1 forward	TTCTGCCGTTCAAGGTTTGG	This study
YGP1 reverse	TAGGTAACCAGCACCCACAG	This study

Although the histone protein level changes were moderate in young histone gene deletion cells, even when cells were synchronized, changes in chromatin compaction, as revealed by MNase digestion patterns, were significant and commensurate with the histone dosage (Fig. 2E). These changes in chromatin organization led to transcriptional silencing defects, which were more substantial in the major H3-H4 copy deletion strain (Fig. 2, F to H). These observations were consistent with the broader transcriptomic changes detected in the major copy deletion strain compared to the minor copy deletion mutant (fig. S2A).

Both the minor and the major copy histone gene deletions resulted in transcriptional responses similar to those induced by mutations resulting in chromatin defects (Fig. 5D). These common changes represented a previously unrecognized stress response form, which we referred to as the CAD or CAD response. DNA damage resistance is consistent with the CAD response. A previous report has shown that histone deletion mutants are more resistant to DNA damage (*9*), which, although unexpected, is consistent with stress response state and inhibition of TOR signaling (*41*).

We found the relationship between histone gene dosage and RLS to be particularly interesting and unexpected. According to a previous literature (*4*), a moderate but not severe reduction of histone dosage (Fig. 1A) could lead to robust life-span extension. The correlation between histone gene dosage and RLS is thus not linear but shows a bipolar distribution (Fig. 6I). Note that the mechanisms for life-span extension by histone overexpression and moderate histone dosage reduction are different, as evidenced by distinct transcriptome profiles (fig. S2D).

Furthermore, we noted dosage-dependent life-span changes when the histone H3-H4 dosage falls between 85 and 15% of the WT. Given the similar transcriptomic response (fig. S2, A and B) and metabolic phenotypes (Fig. 5, A and B) between *htf1*Δ and *htf2*Δ, which is also evidenced by the very similar transcriptomic changes, it is possible that the level of the CAD response is maxed out by 85% histone dosage in *htf1*Δ. Hence, with increasing chromatin defects when further reducing histone dosage, longevity benefits start to shrink, reaching the WT level at 30% histone dosage in *htf2*Δ *HTF1OE* (fig. S1C), and hence shorter life span than the WT at 15% histone dosage in *htf2*Δ (Fig. 1A).

Inhibition of TOR signaling links the CAD response to longevity

Most CAD mutants, including those inactivated in the major copy of the H3-H4 gene pair and in the histone chaperone Asf1, are short-lived (*4*) . The unexpected robust longevity of the minor copy H3-H4 deletion *htf1*Δ led to the characterization of the CAD, which, upon moderate activation, can induce a hormetic state that promotes longevity. Many of the previously identified long-lived mutants show various forms of increased stress response (*42*, *43*). Considering that the defects observed in *hft1*Δ were more moderate than those in *htf2*Δ, the activated CAD response likely compensates for the moderate defects in *htf1*Δ, constituting a hormetic response.

Notably, TOR inhibition was found to be required for the longevity phenotype of *htf1*Δ but not for the transcriptional response. Hence, the activation of CAD response genes likely inhibits TOR signaling, thereby promoting longevity. Despite previous work proposing a relationship between TOR signaling and hormesis (*44*), little evidence exists to support the link between the two. We believe that this study provides one example showing that the activation of TOR signaling

Table 3. Yeast strains used in this study.

Strain name	Genotype	Source
YWD2000	*his3-200 leu2Δ1 ura3-52 trp1Δ63 lys2-128*	This study
YWD1000	*MATa his3-200 leu2Δ1 ura3-52 trp1Δ63 lys2-128 (hht1-hhf1)Δ::LEU2*	This study
YWD200	*MATa his3-200 leu2Δ1 ura3-52 trp1Δ63 lys2-128 (hht2-hhf2)Δ::HIS3*	This study
RYY111	*MATa (hta2-htb2)Δ::TRP1 lys2-128 leu2Δ1 ura3-52 trp1Δ63 his3Δ200*	This study
RYY79	*YWD1000 HHT1-HHF1-URA3*	This study
RYY83	*YWD200 HHT2-HHF2-URA3*	This study
BY4741	*MATa his3Δ1 leu2Δ0 met15Δ0 ura3Δ0*	Thermo Fisher Scientific
YKO3145	*BY4741 hht1Δ::kanMX4*	Thermo Fisher Scientific
YKO5357	*BY4741 hht2Δ::kanMX4*	Thermo Fisher Scientific
YKO3144	*BY4741 hhf1Δ::kanMX4*	Thermo Fisher Scientific
YKO5356	*BY4741 hhf2Δ::kanMX4*	Thermo Fisher Scientific
RYY81	*YWD2000 HHT2-HHF2-URA3*	This study
RYY92	*YWD2000 S31Δ::kanMX4*	This study
RYY93	*YWD1000 snf1Δ::kanMX4*	This study
RYY94	*YWD200 snf1Δ::kanMX4*	This study
RYY95	*YWD2000 fob1Δ::kanMX4 sir2Δ::URA3*	This study
RYY96	*YWD1000 fob1Δ::kanMX4 sir2Δ::URA3*	This study
RYY47	*YWD2000 tor1Δ::kanMX4*	This study
RYY39	*YWD1000 tor1Δ::kanMX4*	This study
RYY57	*YWD2000 rpl20bΔ::kanMX4*	This study
RYY58	*YWD1000 rpl20bΔ::kanMX4*	This study
RYY109	*YWD2000 TOR1 L2134 M*	This study
RYY110	*YWD1000 TOR1 L2134 M*	This study
YKO1310	*BY4741 asf1Δ::kanMX4*	Thermo Fisher Scientific
YKO3335	*BY4741 msi1Δ::kanMX4*	Thermo Fisher Scientific
YKO2006	*BY4741 rtt106Δ::kanMX4*	Thermo Fisher Scientific
RYY114	*YWD2000 msn2Δ::kanMX4*	This study
RYY115	*YWD1000 msn2Δ::kanMX4*	This study
RYY124	*YWD2000 gis1Δ::kanMX4*	This study
RYY125	*YWD2000 hot1Δ::kanMX4*	This study
RYY126	*YWD1000 gis1Δ::kanMX4*	This study
RYY127	*YWD1000 hot1Δ::kanMX4*	This study
RYY300	*YWD2000 SIR2-URA3*	This study
RYY301	*YWD1000 SIR2-URA3*	This study
RYY302	*YWD2000 MSN2-URA3*	This study
RYY303	*YWD1000 MSN2-URA3*	This study
RYY304	*YWD2000 GIS1-URA3*	This study
RYY305	*YWD1000 GIS1-URA3*	This study

prepares cells for rapid growth under optimal conditions, whereas inhibition of TOR pathways places cells in a stress response state and promotes survival rather than proliferation, thus benefiting longevity.

Response to CADs in higher eukaryotes

The fundamental chromatin structure and the underlying regulatory mechanisms are highly conserved among eukaryotes. Certain aging-associated changes in chromatin structure, such as histone loss and heterochromatin defects, are also common among different eukaryotic models (*2*). Therefore, we investigated whether the CAD response we discovered in yeast is conserved in other eukaryotes. Existing RNA-seq datasets from several genetic models that resemble the yeast CAD mutants were selected for analysis. These models include reduced histone copy mutants in *D. melanogaster*, moderate H2A knockdown in *C. elegans*, and knockdown of the p150 subunit of histone chaperone CAF-1 in MES cells. Analysis of these transcriptomic datasets has identified a potential CAD response signature, represented by down-regulated TOR signaling and protein synthesis (Fig. 5, E to H). Moreover, similarly to the yeast *htf1*Δ strain, the H2A knockdown worm was found to have a longer life span (*25*). These findings suggest that the CAD response and CAD-mediated longevity may be conserved among higher eukaryotes. Therefore, our discovery may offer new targets for aging intervention and approaches for promoting longevity.

MATERIALS AND METHODS

Yeast RLS

A microfluidic platform was used to record replicative aging of single yeast cells, as described by (*45*), using the Invitrogen EVOS FL Auto Imaging System. Briefly, cells were grown overnight in filter-sterilized yeast extract, peptone, and dextrose (YPD) medium, diluted 20-fold with fresh medium, and loaded onto a microfluidic chip. Medium flow speed was set at 10 μl/min, and pictures were taken at 10-min intervals for 65 to 72 hours.

Yeast growth test on solid media

Yeast cells were grown overnight at 30°C, diluted to optical density at 600 nm (OD_{600}) of ~0.1, and spotted in fivefold serial dilutions on designated agar plates. Plates were incubated at 30°C for 24 hours for the YPD plate or 48 hours for the drug plate. Plates were then imaged using the Epson Perfection V500 Photo scanner.

Protein extraction and quantitative Western blot analysis

Yeast cells were harvested at an OD_{600} of 0.8 to 1.0 by centrifugation at 3000 rpm for 3 min and stored at −80°C until further processing. Cells were lysed in lysis buffer [50 mM tris-HCl, 300 mM NaCl, 1 mM EDTA, 1 mM NP-40, 10% glycerol, 1 mM phenylmethylsulfonyl fluoride, and 1× protease inhibitor cocktail (Pierce) by bead beating with zirconia/silica beads (Biospec) using 6 cycles of alternating 1-min beating and 2-min pause on ice, using a BioSpec Minibead-beater]. This was followed by sonication at 50% amplitude for 10 min (30 s on/30 s off cycles) using the EpiShear Multi-Sample Sonicator (Active Motif). Following centrifugation, total protein was diluted to a concentration of 1 mg/ml in lysis buffer, denatured with 1× Bolt LDS Sample Buffer and Sample Reducing Agent at 65°C for 10 min, and separated using a Bolt 4 to 12% Bis-Tris Plus Gel (Thermo Fisher Scientific). The transfer process was performed overnight in Towbin buffer [25 mM tris, 192 mM glycine (pH 8.3), and 20% methanol] at 20 V. Primary antibody was added at the final concentration of

1 mg/ml and incubated overnight at 4°C, with subsequent secondary antibody (0.1 mg/ml) incubation for 1 hour. The Odyssey CLx Scanning System (LI-COR Biosciences) and Image Studio Lite Ver5.2 software were used for membrane scanning and image quantification using the average density method. At least three biological repeats were included for quantification unless otherwise indicated. Antibodies used in this project were listed in Table 1.

MNase digestion and gel analysis

Yeast cells, harvested at OD_{600} of 0.8 to 1.0, were cross-linked with 2% (v/v) of 37% formaldehyde for 30 min, followed by quenching of the reaction with 125 mM glycine. The cells were then washed once with dH_2O, followed by spheroblasting with Zymolase 20T in buffer Z (1 M sorbitol and 50 mM tris-HCl at pH 7.5) for 30 min. All digested samples were verified to have an OD_{600} less than 20% of the starting material. Samples were then treated with indicated concentrations of MNase at 37°C in NP buffer (1 M sorbitol, 50 mM NaCl, 10 mM tris-HCl at pH 7.4, 5 mM $MgCl_2$, 1 mM $CaCl_2$, 0.075% IGEPAL CA-630, and 500 μM spermidine). Reactions were stopped after 20 min using 5× STOP buffer (5% SDS and 50 mM EDTA). RNA was removed with addition of 20 μl of ribonuclease (RNase; 10 mg/ml) per reaction and incubation for 1 hour at 37°C. Following the addition of 4 μl of proteinase K (20 mg/ml), the samples were incubated overnight at 65°C to reverse the cross-linking. Samples were extracted with 1 volume of phenol/chloroform–indole-3-acetic acid and centrifuged at room temperature for 15 min. DNA was precipitated by adding 1 volume of 2-propanol, washed with 70% ethanol, and resuspended in 100 μl of water. DNA samples were quantified by the Qubit double-stranded DNA (dsDNA) HS Assay Kit (Thermo Fisher Scientific) with Qubit Fluorometer (Thermo Fisher Scientific) and diluted to the same concentration. Gel electrophoresis was carried out on a 1.5% agarose gels prestained with SYBR safe (Thermo Fisher Scientific) and visualized by ChemiDoc XRS+ Imaging system (Bio-Rad). Quantitative analysis was performed using the Quantity One 1-D Analysis Software (Bio-Rad).

Measuring α-factor responsiveness and cell cycle synchronization

Mid-log phase yeast cells with an OD_{600} of 0.6 to 0.8 were used for the experiment. YPD agar medium containing α-factor was added at designated concentration to Lab-Tek II chambers (Thermo Fisher Scientific) and allowed it to solidify and dry at room temperature for 1 day. The image capture process was performed, as described by (*46*), using the 10× objective of the Invitrogen EVOS FL Auto Imaging System, with bright-field images captured every 10 min for 8 hours. Cells that showed visible mating projection within the first two cell cycles were counted as responsive to α-factor.

For cell cycle synchronization, overnight cultures were diluted to OD_{600} = 0.3. Following the incubation of the cells with 10 μM α-factor at 30°C for 1 hour, a second dose of 10 μM α-factor was added. Cell morphology was examined using a 40× objective lens of ZEISS Primo Star microscope to assess the arrest efficiency. Synchronized cells were released by washing and resuspending in YPD medium, and samples were harvested at indicated time points.

RNA extraction, reverse transcription PCR, and real-time qPCR analysis

Yeast cells were lysed in QIAzol buffer (QIAGEN) by 4 cycles (1 min on, 2 min pause on ice) of bead beating with 0.5-mm zirconia/silica beads (BioSpec). Total RNA was purified using the miRNeasy Mini Kit (QIAGEN). Reverse transcription was performed using the High-Capacity cDNA Reverse Transcription Kit (Thermo Fisher Scientific) with 1 μg of purified RNA. Quantitative real-time PCR was performed using the ViiA 7 Real-Time PCR System (Thermo Fisher Scientific) and analyzed using the QuantStudio Real-Time PCR software. Yeast gene expression data were normalized to the *ACT1* housekeeping control. All qPCR primers used are listed in Table 2.

Whole-cell DNA extraction

Yeast cells, grown overnight in YPD, were collected by centrifugation at 3000*g*. Zymolase digestion was conducted in buffer I [1 M sorbitol and 0.1 M EDTA-Na_2 (pH7.5)] containing Zymolyase T20 (0.02 U/μl) at 37°C. Following a 60-min incubation with the zymolyase and subsequent addition of 50 μl of buffer II [50 mM tris-HCl, 20 mM EDTA-Na_2, and 0.35 M SDS (pH 7.4)], the cells were incubated at 65°C for 5 min. Precipitation was performed by adding 5 M potassium acetate and placing the samples at −20°C for 10 min, followed by a 15-min centrifugation at 4°C and 15,000 rpm. Following the treatment of the supernatants with 5 μl of RNase (10 mg/ml) for 1 hour at 37°C and the addition of 1 volume of 2-propanol, the samples were incubated at room temperature for 5 min. Nucleic acid pellets were collected by centrifugation for 15 min at 4°C and 15,000 rpm, washed with 70% ethanol, and air-dried at room temperature for 10 min. Pellets were resuspended in 100 μl 1× TE [10 mM tris-HCl (pH 8.0) and 1 mM EDTA].

RNA-seq and MNase-seq library preparation and next-generation sequencing

Total RNA was extracted as described above. Poly-A RNA was purified from 5 μg total RNA with Dynabeads Oligo $(dT)_{25}$ (Thermo Fisher Scientific). Paired-end RNA libraries were prepared using the NEBNext Ultra Directional RNA Library Prep Kit for Illumina (New England BioLabs). Sequencing of three biological replicates was performed using the Illumina HiSeq 2500 platform.

Chromatin was digested with 120 U of MNase (New England BioLabs) and 8 U of EXOIII (Promega), as previously described (*47*), and purified using the QIAGEN Genomic-tip 20/G column. Mononucleosome DNA was separated by agarose gel electrophoresis and purified using the Quantum Prep Freeze 'N Squeeze DNA Gel Extraction Spin Column (Bio-Rad). Purified DNA was treated with NEBNext End Repair Module, followed by Agencourt AMPure XP beads (Beckman Coulter) cleanup, and dA (deoxyadenosine) tailing with Klenow fragment (New England BioLabs). After purification, the samples were ligated with Illumina TruSeq multiplexing primers using the Quick Ligation Kit (New England BioLabs) and amplified using the KAPA HiFi Ready Mix (Thermo Fisher Scientific). Following the final purification, the DNA was quantified using the Qubit dsDNA HS Assay Kit (Thermo Fisher Scientific). Sequencing was performed on the Illumina HiSeq 2500 platform using three biological replicates.

Cell cycle analysis by flow cytometry

Yeast cells were harvested at OD_{600} of 0.6 to 0.8, fixed with cold 70% ethanol, and kept at 4°C until further use. Cells were washed twice with phosphate-buffered saline (PBS) (Dulbecco) and then treated with RNase (1 mg/ml) at 37°C for 2 hours. Following the addition of 100 μl of a propidium iodide solution (0.05 mg/ml), the samples were incubated overnight at 4°C. Following the addition of 900 μl of PBS to the samples, flow cytometry was performed using the LSRFortessa

cell analyzer (BD Biosciences). Flow cytometry data analysis was performed using FlowJo software.

ATP level measurement

Yeast cells were incubated in synthetic complete (SC) medium (0.5% ammonium sulfate, 0.17% yeast nitrogen base without amino acids and ammonium sulfate, 0.2% SC mix, and 2% dextrose) to an OD_{600} of 0.6 to 0.8. Samples were harvested by centrifugation at 3000*g* and adjusted to contain the same number of cells. Approximately 10^6 cells were added per well of a 96-well opaque plate. The BacTiter-Glo reagent (Promega) was added to each sample (100 µl per well) and mixed for 2 min before the experiment. To minimize the impact of cell wall structure on lysis efficiency, luminescence intensity was read five times in 2-min intervals, with the highest read within the 10-min experimental period used for analysis. Luminescence measurements were performed using the BioTek Synergy 2 Multi-Mode Reader, with the data analyzed using the Gen5 software. Two biological replicates were used for these experiments.

Isolation of young and old yeast cells

Young and old yeast cells were purified using a biotin-based method, as previously described (*16*). Yeast cells were harvested at OD_{600} ~1.0, washed with PBS, and labeled for 15 min at 30°C with EZ-Link Biotin (Thermo Fisher Scientific) at a concentration of 1 mg/10^8 cells. The cells were then washed three times with PBS containing 0.1 M glycine to quench the labeling reaction and remove free biotin, followed by resuspension in SC medium for incubation overnight. The cells were harvested at an OD_{600} of 1.2 to 1.6, resuspended in PBS + BE [PBS with BSA (1 mg/ml) and 2 mM EDTA], and incubated with the Dynabeads Biotin Binder (Thermo Fisher Scientific) at 4°C for 1 hour with shaking. Before this, the Dynabeads Biotin Binder was washed and resuspended in PBS + BE. The supernatant of the first wash was kept as the young cell control. After washing five times with PBS, the beads were resuspended in PBS for further analysis. Young and old cells (10 µl) were fixed using 1 µl of 37% formaldehyde for bud scar counting. Protein samples were treated as indicated in Western blot section, and due to technical limitation, three technical replicates were used to quantify protein level.

Bioinformatics and data analysis

RNA-seq data processing and transcriptome analysis

Read alignment was performed using TopHat2 (*48*) with the default settings. Read counting and gene expression analysis was done using htseq-count (*49*) and edgeR (*50*). Transcriptome analysis was based on $\log_2$ fold change calculated using edgeR from three biological replicates. All significantly up- or down-regulated genes with false discovery rate < 0.01 were selected for downstream analysis. For published MES transcriptome datasets, GO analysis of biological process enrichment was performed with the DAVID Functional Annotation Tool (https://david.ncifcrf.gov/), using the GOTERM_BP_DIRECT option. For all GO analyses, default settings were used, and categories with a Benjamini-Hochberg $P < 0.05$ were considered as significantly enriched. Transcriptome clustering analysis with a previous transcriptomic dataset (*32*) was performed using a *k*-means algorithm and R. List of effectors of transcription factors were retrieved through the Yeastract website (*51*), with the "TF acting as activator" and "DNA binding plus expression evidence" options. A heat diffusion constant of 0.25 was used for the TF rank algorithm to calculate weight of transcription factor. Motif analysis was performed by Homer software (*52*) with de novo motif analysis. List of all nonsignificantly up-regulated genes in *htf1*Δ was used as background.

MNase-seq data processing and nucleosome profile analysis

Read alignment was performed using Bowtie2 (*53*). Nucleosome calling and occupancy calculations were performed using Danpos2 (*54*). Statistical significance of the differences between two nucleosome profiles was calculated using the perturbation test. Relative nucleosome scores across the designated regions were calculated for the control and test groups, followed by subtraction of the values. This value was recorded as the difference in nucleosome occupancy. The nucleosome difference score was calculated 1000 times on randomly selected regions. The *P* value was defined as the possibility that random promoters have a larger nucleosome difference score than the test group. MNase-seq tracks for individual genes were visualized by the Integrative Genomics Viewer (*55*).

Statistics

Significance of gene group overlap was calculated on the basis of hypergeometric distribution. Yeast RLS and cell cycle time *P* values were determined using the Wilcoxon rank-sum test. Enrichment of GO categories was calculated using the χ^2 test. Statistical significance of all other data not specified above was calculated using an unpaired equal variance two-tailed Student's *t* test.

Yeast strains and media

All strains used in this study are listed in Table 3. The yeast strain YWD2000 was used as the parent strain for all histone mutation–containing strains and designated as the WT. Other single gene deletion strains were in the BY4741 parental background. Standard YPD medium (1% yeast extract, 2% peptone, and 2% glucose, with 1.5% agar included for solid medium) was used for all yeast experiments, except as noted. All strains were constructed by transformation.

SUPPLEMENTARY MATERIALS

Supplementary material for this article is available at http://advances.sciencemag.org/cgi/content/full/5/7/eaav1165/DC1

Fig. S1. Characterization of histone deletion strains.
Fig. S2. Transcriptome analysis of *htf2*Δ and *HTF2OE* strains.
Fig. S3. Molecular pathway analysis of histone deletion genes.
Fig. S4. Stress response factors connect CAD to longevity.
Table S1. All RNA-seq data used in this study.
Table S2. All Venn diagram gene lists used in this study.
Table S3. Correlation analysis between *htf1*Δ and yeast single gene deletion dataset (*31*).
Table S4. Transcription factors of which targets were enriched among genes up-regulated in *htf1*Δ.
Table S5. Msn2- and Gis1-regulated genes significantly up-regulated in *htf1*Δ.
Table S6. Statistics of all RLS experiments in this study.

REFERENCES AND NOTES

1. O. Bell, V. K. Tiwari, N. H. Thomä, D. Schübeler, Determinants and dynamics of genome accessibility. *Nat. Rev. Genet.* **12**, 554–564 (2011).
2. S. Pal, J. K. Tyler, Epigenetics and aging. *Sci. Adv.* **2**, e1600584 (2016).
3. P. Oberdoerffer, An age of fewer histones. *Nat. Cell Biol.* **12**, 1029–1031 (2010).
4. J. Feser, D. Truong, C. Das, J. J. Carson, J. Kieft, T. Harkness, J. K. Tyler, Elevated histone expression promotes life span extension. *Mol. Cell* **39**, 724–735 (2010).
5. S. D. L. Postnikoff, J. E. Johnson, J. K. Tyler, The integrated stress response in budding yeast lifespan extension. *Microb. Cell* **4**, 368–375 (2017).
6. S. L. Cross, M. M. Smith, Comparison of the structure and cell cycle expression of mRNAs encoded by two histone H3-H4 loci in *Saccharomyces cerevisiae*. *Mol. Cell. Biol.* **8**, 945–954 (1988).
7. M. M. Smith, V. B. Stirling, Histone H3 and H4 gene deletions in *Saccharomyces cerevisiae*. *J. Cell Biol.* **106**, 557–566 (1988).

8. D. E. Libuda, F. Winston, Alterations in DNA replication and histone levels promote histone gene amplification in *Saccharomyces cerevisiae*. *Genetics* **184**, 985–997 (2010).
9. D. Liang, S. L. Burkhart, R. K. Singh, M.-H. Kabbaj, A. Gunjan, Histone dosage regulates DNA damage sensitivity in a checkpoint-independent manner by the homologous recombination pathway. *Nucleic Acids Res.* **40**, 9604–9620 (2012).
10. M. A. McCormick, A. G. Mason, S. J. Guyenet, W. Dang, R. M. Garza, M. K. Ting, R. M. Moller, S. L. Berger, M. Kaeberlein, L. Pillus, A. R. La Spada, B. K. Kennedy, The SAGA histone deubiquitinase module controls yeast replicative lifespan via Sir2 interaction. *Cell Rep.* **8**, 477–486 (2014).
11. S.-i. Imai, C. M. Armstrong, M. Kaeberlein, L. Guarente, Transcriptional silencing and longevity protein Sir2 is an NAD-dependent histone deacetylase. *Nature* **403**, 795–800 (2000).
12. J. R. Delaney, G. L. Sutphin, B. Dulken, S. Sim, J. R. Kim, B. Robison, J. Schleit, C. J. Murakami, D. Carr, E. H. An, E. Choi, A. Chou, M. Fletcher, M. Jelic, B. Liu, D. Lockshon, R. M. Moller, D. N. Pak, Q. Peng, Z. J. Peng, K. M. Pham, M. Sage, A. Solanky, K. K. Steffen, M. Tsuchiya, S. Tsuchiyama, S. Johnson, C. Raabe, Y. Suh, Z. Zhou, X. Liu, B. K. Kennedy, M. Kaeberlein, Sir2 deletion prevents lifespan extension in 32 long-lived mutants. *Aging Cell* **10**, 1089–1091 (2011).
13. S. Wullschleger, R. Loewith, M. N. Hall, TOR signaling in growth and metabolism. *Cell* **124**, 471–484 (2006).
14. K. K. Steffen, V. L. MacKay, E. O. Kerr, M. Tsuchiya, D. Hu, L. A. Fox, N. Dang, E. D. Johnston, J. A. Oakes, B. N. Tchao, D. N. Pak, S. Fields, B. K. Kennedy, M. Kaeberlein, Yeast life span extension by depletion of 60s ribosomal subunits is mediated by Gcn4. *Cell* **133**, 292–302 (2008).
15. T. Takahara, T. Maeda, Transient sequestration of TORC1 into stress granules during heat stress. *Mol. Cell* **47**, 242–252 (2012).
16. W. Dang, G. L. Sutphin, J. A. Dorsey, G. L. Otte, K. Cao, R. M. Perry, J. J. Wanat, D. Saviolaki, C. J. Murakami, S. Tsuchiyama, B. Robison, B. D. Gregory, M. Vermeulen, R. Shiekhattar, F. B. Johnson, B. K. Kennedy, M. Kaeberlein, S. L. Berger, Inactivation of yeast Isw2 chromatin remodeling enzyme mimics longevity effect of calorie restriction via induction of genotoxic stress response. *Cell Metab.* **19**, 952–966 (2014).
17. P. Capy, G. Gasperi, C. Biémont, C. Bazin, Stress and transposable elements: Co-evolution or useful parasites? *Heredity* **85**, 101–106 (2000).
18. W. Hilt, D. H. Wolf, Stress-induced proteolysis in yeast. *Mol. Microbiol.* **6**, 2437–2442 (1992).
19. A. P. Gasch, P. T. Spellman, C. M. Kao, O. Carmel-Harel, M. B. Eisen, G. Storz, D. Botstein, P. O. Brown, Genomic expression programs in the response of yeast cells to environmental changes. *Mol. Biol. Cell* **11**, 4241–4257 (2000).
20. F. Abe, Induction of DAN/TIR yeast cell wall mannoprotein genes in response to high hydrostatic pressure and low temperature. *FEBS Lett.* **581**, 4993–4998 (2007).
21. X. Ye, A. A. Franco, H. Santos, D. M. Nelson, P. D. Kaufman, P. D. Adams, Defective S phase chromatin assembly causes DNA damage, activation of the S phase checkpoint, and S phase arrest. *Mol. Cell* **11**, 341–351 (2003).
22. D. D'Amours, S. P. Jackson, The MRE11 complex: At the crossroads of DNA repair and checkpoint signalling. *Nat. Rev. Mol. Cell Biol.* **3**, 317–327 (2002).
23. G. Basile, M. Aker, R. K. Mortimer, Nucleotide sequence and transcriptional regulation of the yeast recombinational repair gene RAD51. *Mol. Cell. Biol.* **12**, 3235–3246 (1992).
24. J. K. Tyler, C. R. Adams, S.-R. Chen, R. Kobayashi, R. T. Kamakaka, J. T. Kadonaga, The RCAF complex mediates chromatin assembly during DNA replication and repair. *Nature* **402**, 555–560 (1999).
25. O. Matilainen, M. S. B. Sleiman, P. M. Quiros, S. M. D. A. Garcia, J. Auwerx, The chromatin remodeling factor ISW-1 integrates organismal responses against nuclear and mitochondrial stress. *Nat. Commun.* **8**, 1818 (2017).
26. R. D. Martinus, G. P. Garth, T. L. Webster, P. Cartwright, D. J. Naylor, P. B. Høj, N. J. Hoogenraad, Selective induction of mitochondrial chaperones in response to loss of the mitochondrial genome. *Eur. J. Biochem.* **240**, 98–103 (1996).
27. I. Tirosh, N. Barkai, Two strategies for gene regulation by promoter nucleosomes. *Genome Res.* **18**, 1084–1091 (2008).
28. K. S. Cho, L. I. Elizondo, C. F. Boerkoel, Advances in chromatin remodeling and human disease. *Curr. Opin. Genet. Dev.* **14**, 308–315 (2004).
29. A. Aguilera, B. Gómez-González, Genome instability: A mechanistic view of its causes and consequences. *Nat. Rev. Genet.* **9**, 204–217 (2008).
30. L. Galdieri, T. Zhang, D. Rogerson, A. Vancura, Reduced histone expression or a defect in chromatin assembly induces respiration. *Mol. Cell. Biol.* **36**, 1064–1077 (2016).
31. A. J. Gossett, J. D. Lieb, In vivo effects of histone H3 depletion on nucleosome occupancy and position in *Saccharomyces cerevisiae*. *PLOS Genet.* **8**, e1002771 (2012).
32. P. Kemmeren, K. Sameith, L. A. L. van de Pasch, J. J. Benschop, T. L. Lenstra, T. Margaritis, E. O'Duibhir, E. Apweiler, S. van Wageningen, C. W. Ko, S. van Heesch, M. M. Kashani, G. Ampatziadis-Michailidis, M. O. Brok, N. A. C. H. Brabers, A. J. Miles, D. Bouwmeester, S. R. van Hooff, H. van Bakel, E. Sluiters, L. V. Bakker, B. Snel, P. Lijnzaad, D. van Leenen, M. J. A. Groot Koerkamp, F. C. P. Holstege, Large-scale genetic perturbations reveal regulatory networks and an abundance of gene-specific repressors. *Cell* **157**, 740–752 (2014).
33. T. J. R. Penke, D. J. McKay, B. D. Strahl, A. G. Matera, R. J. Duronio, Direct interrogation of the role of H3K9 in metazoan heterochromatin function. *Genes Dev.* **30**, 1866–1880 (2016).
34. D. J. McKay, J. D. Lieb, A common set of DNA regulatory elements shapes *Drosophila* appendages. *Dev. Cell* **27**, 306–318 (2013).
35. C. Mayer, I. Grummt, Ribosome biogenesis and cell growth: mTOR coordinates transcription by all three classes of nuclear RNA polymerases. *Oncogene* **25**, 6384–6391 (2006).
36. T. Ishiuchi, R. Enriquez-Gasca, E. Mizutani, A. Bošković, C. Ziegler-Birling, D. Rodriguez-Terrones, T. Wakayama, J. M. Vaquerizas, M.-E. Torres-Padilla, Early embryonic-like cells are induced by downregulating replication-dependent chromatin assembly. *Nat. Struct. Mol. Biol.* **22**, 662–671 (2015).
37. A. Bulut-Karslioglu, S. Biechele, H. Jin, T. A. Macrae, M. Hejna, M. Gertsenstein, J. S. Song, M. Ramalho-Santos, Inhibition of mTOR induces a paused pluripotent state. *Nature* **540**, 119–123 (2016).
38. I. Tirosh, A. Weinberger, M. Carmi, N. Barkai, A genetic signature of interspecies variations in gene expression. *Nat. Genet.* **38**, 830–834 (2006).
39. M. Wei, P. Fabrizio, J. Hu, H. Ge, C. Cheng, L. Li, V. D. Longo, Life span extension by calorie restriction depends on rim15 and transcription factors downstream of Ras/PKA, Tor, and Sch9. *PLOS Genet.* **4**, e13 (2008).
40. D. J. McKay, S. Klusza, T. J. R. Penke, M. P. Meers, K. P. Curry, S. L. McDaniel, P. Y. Malek, S. W. Cooper, D. C. Tatomer, J. D. Lieb, B. D. Strahl, R. J. Duronio, A. G. Matera, Interrogating the function of metazoan histones using engineered gene clusters. *Dev. Cell* **32**, 373–386 (2015).
41. R. Loewith, M. N. Hall, Target of Rapamycin (TOR) in nutrient signaling and growth control. *Genetics* **189**, 1177–1201 (2011).
42. D. Gems, L. Partridge, Stress-response hormesis and aging: "that which does not kill us makes us stronger". *Cell Metab.* **7**, 200–203 (2008).
43. J. K. Tyler, J. E. Johnson, The role of autophagy in the regulation of yeast life span. *Ann. N. Y. Acad. Sci.* **1418**, 31–43 (2018).
44. M. V. Blagosklonny, Hormesis does not make sense except in the light of TOR-driven aging. *Aging* **3**, 1051–1062 (2011).
45. M. C. Jo, W. Liu, L. Gu, W. Dang, L. Qin, High-throughput analysis of yeast replicative aging using a microfluidic system. *Proc. Natl. Acad. Sci. U.S.A.* **112**, 9364–9369 (2015).
46. G. Schlissel, M. K. Krzyzanowski, F. Caudron, Y. Barral, J. Rine, Aggregation of the Whi3 protein, not loss of heterochromatin, causes sterility in old yeast cells. *Science* **355**, 1184–1187 (2017).
47. I. Whitehouse, O. J. Rando, J. Delrow, T. Tsukiyama, Chromatin remodelling at promoters suppresses antisense transcription. *Nature* **450**, 1031–1035 (2007).
48. D. Kim, G. Pertea, C. Trapnell, H. Pimentel, R. Kelley, S. L. Salzberg, TopHat2: Accurate alignment of transcriptomes in the presence of insertions, deletions and gene fusions. *Genome Biol.* **14**, R36 (2013).
49. S. Anders, P. T. Pyl, W. Huber, HTSeq—A Python framework to work with high-throughput sequencing data. *Bioinformatics* **31**, 166–169 (2015).
50. M. D. Robinson, D. J. McCarthy, G. K. Smyth, edgeR: A bioconductor package for differential expression analysis of digital gene expression data. *Bioinformatics* **26**, 139–140 (2009).
51. M. C. Teixeira, P. Monteiro, P. Jain, S. Tenreiro, A. R. Fernandes, N. P. Mira, M. Alenquer, A. T. Freitas, A. L. Oliveira, I. Sá-Correia, The YEASTRACT database: A tool for the analysis of transcription regulatory associations in *Saccharomyces cerevisiae*. *Nucleic Acids Res.* **34**, D446–D451 (2006).
52. S. Heinz, C. Benner, N. Spann, E. Bertolino, Y. C. Lin, P. Laslo, J. X. Cheng, C. Murre, H. Singh, C. K. Glass, Simple combinations of lineage-determining transcription factors prime *cis*-regulatory elements required for macrophage and B cell identities. *Mol. Cell* **38**, 576–589 (2010).
53. B. Langmead, S. L. Salzberg, Fast gapped-read alignment with Bowtie 2. *Nat. Methods* **9**, 357–359 (2012).
54. K. Chen, Y. Xi, X. Pan, Z. Li, K. Kaestner, J. Tyler, S. Dent, X. He, W. Li, DANPOS: Dynamic analysis of nucleosome position and occupancy by sequencing. *Genome Res.* **23**, 341–351 (2013).
55. J. T. Robinson, H. Thorvaldsdóttir, W. Winckler, M. Guttman, E. S. Lander, G. Getz, J. P. Mesirov, Integrative genomics viewer. *Nat. Biotechnol.* **29**, 24–26 (2011).

Acknowledgments: We appreciate G. Ira for helpful advices on this manuscript. We also thank G. Ira, M. Wang, A. Catic, and A. Bertuch for useful discussion during this study. **Funding:** This study was supported by NIH grants R00AG037646, R01AG052507, R42AG058368, and CPRIT award R1306 to W.D., and BCM Cullen Scholarship to R.Y. **Author contributions:** Conceptualization: R.Y. and W.D. Data curation: R.Y. and Y.S. Formal analysis: R.Y., L.S., and W.D. Funding acquisition: L.Q. and W.D. Investigation: R.Y. Methodology: R.Y., L.S., and

W.D. Project administration: R.Y. and W.D. Resources: X.H., L.Q., and W.D. Supervision: W.D. Validation: R.Y. and W.D. Writing (original draft): R.Y. and W.D. Writing (review and editing): R.Y., L.S., Y.S., X.H., L.Q., and W.D. **Competing interests:** The authors declare that they have no competing interests. **Data and materials availability:** All data needed to evaluate the conclusions in the paper are present in the paper and/or the Supplementary Materials. All next-generation sequencing data are available at NCBI BioProject accession number PRJNA436398. Additional data related to this paper may be requested from the authors.

Submitted 15 August 2018
Accepted 30 May 2019
Published 10 July 2019
10.1126/sciadv.aav1165

Citation: R. Yu, L. Sun, Y. Sun, X. Han, L. Qin, W. Dang, Cellular response to moderate chromatin architectural defects promotes longevity. *Sci. Adv.* **5**, eaav1165 (2019).

Cellular response to moderate chromatin architectural defects promotes longevity

Ruofan Yu, Luyang Sun, Yu Sun, Xin Han, Lidong Qin and Weiwei Dang

Sci Adv **5** (7), eaav1165.
DOI: 10.1126/sciadv.aav1165